

The environments of $z \sim 1$ active galactic nuclei at $3.6 \mu\text{m}$

J. T. Falder,^{1*} J. A. Stevens,¹ Matt J. Jarvis,¹ M. J. Hardcastle,¹ M. Lacy,²
R. J. McLure,³ E. Hatziminaoglou,⁴ M. J. Page⁵ and G. T. Richards⁶

¹Centre for Astrophysics Research, University of Hertfordshire, College Lane, Herts AL10 9AB

²Spitzer Science Center, California Institute of Technology, MC 220-6, Pasadena, CA 91125, USA

³SUPA, † Institute for Astronomy, University of Edinburgh, Royal Observatory, Blackford Hill, Edinburgh EH9 3HJ

⁴European Southern Observatory, Karl-Schwarzschild-Str. 2, 85748 Garching bei Munchen, Germany

⁵Mullard Space Science Laboratory, Holmbury St. Mary, Dorking, Surrey RH5 6NT

⁶Department of Physics, Drexel University, Philadelphia, PA 19104, USA

Accepted 2010 January 29. Received 2010 January 29; in original form 2009 December 3

ABSTRACT

We present an analysis of a large sample of active galactic nuclei (AGN) environments at $z \sim 1$ using stacked *Spitzer* data at $3.6 \mu\text{m}$. The sample contains type 1 and type 2 AGN in the form of quasars and radio galaxies, and spans a large range in both optical and radio luminosity. We find, on average, that two to three massive galaxies containing a substantial evolved stellar population lie within a 200–300 kpc radius of the AGN, constituting a $>8\sigma$ excess relative to the field. Secondly, we find evidence for the environmental source density to increase with the radio luminosity of AGN, but not with black hole mass. This is shown first by dividing the AGN into their classical AGN types, where we see more significant overdensities in the fields of the radio-loud AGN. If instead we dispense with the classical AGN definitions, we find that the source overdensity as a function of radio luminosity for all our AGN exhibits a positive correlation. One interpretation of this result is that the Mpc-scale environment is in some way influencing the radio emission that we observe from AGN. This could be explained by the confinement of radio jets in dense environments leading to enhance radio emission or, alternatively, may be linked to more rapid black hole spin brought on by galaxy mergers.

Key words: galaxies: active – galaxies: clusters: general – galaxies: high-redshift – quasars: general – galaxies: statistics.

1 INTRODUCTION

It is now widely accepted that high-luminosity active galactic nuclei (AGN) harbour accreting supermassive black holes implying that their host galaxies are amongst the most massive objects in existence at their respective epochs. Indeed, many studies have now shown that AGN preferentially reside within fields containing overdensities of galaxies (e.g. Hall & Green 1998; Best et al. 2003; Wold et al. 2003; Hutchings, Scholz & Bianchi 2009). Together these points support the idea that AGN can be utilized as signposts to extreme regions of the dark matter density and thus the most massive dark matter haloes (e.g. Ivison et al. 2000; Pentericci et al. 2000; Stevens et al. 2003) at any given epoch. Combining this technique with large multiwavelength surveys, like the Sloan Digital Sky Survey (SDSS; Adelman-McCarthy et al. 2006) which has identified up to 100 000 broad-line quasi-stellar objects (hereafter quasars) up to the highest

measured redshifts (i.e. $z = 6.4$; Fan et al. 2003), has opened up a new era in AGN research.

Many authors have addressed the question of whether the environments of radio-loud AGN, such as radio-loud quasars (RLQs) or radio galaxies (RGs), are any different from those of radio-quiet AGN, such as radio-quiet quasars (RQQs), with conflicting results. The first work that compared directly the environments of RLQs and RQQs was Yee & Green (1984), in which a marginally more significant overdensity was detected around the RLQs in their sample of objects at $0.05 < z < 0.55$. However, a later improved study with more data and refined techniques removed the significance of this result (Yee & Green 1987). More work on the topic was conducted by Ellingson, Yee & Green (1991) who added more faint RQQs to the Yee & Green (1987) sample. As a result they reported a significant difference in the environments preferred by RLQs and RQQs, with RQQs in general preferring poorer environments at the 99 per cent confidence level. At $0.9 < z < 4.2$, Hutchings et al. (1999) found that RLQs occupied more dense environments in the near-infrared than RQQs. In contrast, both Wold et al. (2001) and McLure & Dunlop (2001) found the environments of RLQs and

*E-mail: j.t.falder@herts.ac.uk

†Scottish Universities Physics Alliance.

RQQs to be indistinguishable at $z \sim 0.2$ and at $0.5 < z < 0.8$, respectively. More recently Kauffmann, Heckman & Best (2008) found that radio-loud AGN reside in environments a factor of 2–3 more dense than radio-quiet AGN in a large matched sample of SDSS emission-line AGN in the local Universe. These results present us with a very mixed picture. However, it is probable that many of them suffer in some way from small number statistics and/or significant selection effects. Furthermore, it may be crucial to understand how the AGN and their environments are linked at all redshifts given that large-scale radio-jet activity could enhance (Wiita 2004) or truncate (Rawlings & Jarvis 2004) star formation on the Mpc scale, and hence be a crucial ingredient in semi-analytic models (e.g. Bower et al. 2006; Croton et al. 2006).

It is still not clear exactly what triggers the radio emission we see in radio-loud AGN, and why we do not see similar emission in otherwise comparable radio-quiet AGN. McLure & Jarvis (2004) showed that, on average, RLQs have 45 per cent more massive black holes than RQQs, and that most RLQs have a black hole mass greater than $10^8 M_{\odot}$. These results suggest that in order to be radio loud an AGN requires a certain mass of black hole. However, at any given black hole mass the range of radio luminosities spans several orders of magnitude and there are RQQs which have black holes equally as massive as the RLQs. Thus black hole mass cannot be the only factor that determines radio power; perhaps the environment of the AGN also contributes.

It is also still not fully understood whether there is a true AGN radio power dichotomy (e.g. Lacy et al. 2001; Ivezić et al. 2002; and more recently White et al. 2007; Zamfir, Sulentic & Marziani 2008), and whether the different types of AGN are intrinsically different or whether we just happen to be observing some whilst they are going through a period of radio loudness. Studying the cluster-scale environments of these objects provides a good means of investigating this issue since, if they are identical objects going through different phases then they should have similar environments on these scales. Alternatively, it may be the case that the environment is in some way linked to the differences that we see in the radio properties of AGN.

In this paper we concentrate on a number density analysis of a sample of 173 AGN fields at the single cosmic epoch of $z \sim 1$, splitting the AGN into their classical types (RLQs, RQQs and RGs), as well as looking for trends with radio luminosity and black hole mass. We use 3.6- μm observations allowing us to sample the peak of the rest-frame stellar spectrum thus maximizing our sensitivity to stellar mass. This work presents an analysis of the environments of the largest, most uniformly selected sample of luminous AGN yet assembled at high redshift. In so doing it forms an extension to previous studies of the environments of AGN with lower radio luminosities and at lower redshifts ($z < 0.3$) performed with SDSS data (e.g. Best et al. 2005; Kauffmann et al. 2008).

In Section 2 we give details of our data, in Section 3 we discuss the source extraction, in Section 4 we explain the method of analysis, then in Section 5 we present our results followed by a discussion in Section 6 and a summary of the main conclusions in Section 7. Throughout this paper we have assumed a flat cosmology with $H_0 = 72 \text{ km s}^{-1} \text{ Mpc}^{-1}$, $\Omega_m = 0.3$ and $\Omega_{\Lambda} = 0.7$. All magnitudes are quoted in the AB system.

2 DATA

The data presented in this paper consist of infrared images of 173 AGN taken at 3.6 μm with the Infrared Array Camera (IRAC) camera on board the *Spitzer Space Telescope*. The sample is split into

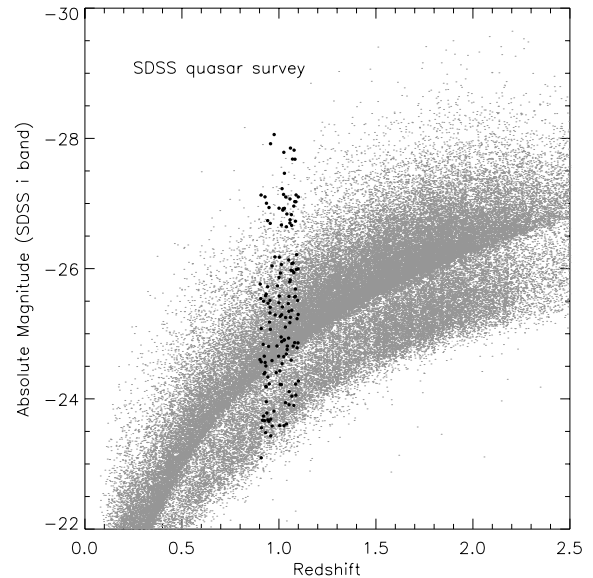


Figure 1. Redshift versus optical absolute magnitude (SDSS *i* band) for quasars from the fifth data release of the SDSS quasar survey (Schneider et al. 2005). The quasars in bold are those used in our sample, clearly showing that we span the 5 mag range in optical luminosity available at $z \sim 1$.

three subsamples, all at the single cosmic epoch of $0.9 < z < 1.1$: 75 RLQs, 71 RQQs and 27 RGs. This redshift was chosen as it is the minimum at which there is a large enough population of high-luminosity quasars to allow comparison with the bright quasars that are observed at higher redshifts. At this redshift the SDSS allows us to sample over 5 mag in quasar optical luminosity (see Fig. 1). This sample thus enables us to decouple luminosity-generated effects from evolutionary ones, something which has plagued many other flux density limited studies in this area. In addition, the targets were chosen to have redshifts optimized, within the chosen range for follow-up CO surveys with interferometers such as the Atacama Large Millimeter Array (ALMA). Observing both unobscured (type 1) AGN, in the form of quasars, and obscured (type 2) AGN, the RGs, allows us to test AGN unification schemes (e.g. Antonucci 1993).

Full details of the quasars will be presented elsewhere (Jarvis et al., in preparation) while a list of the RGs giving their main properties is given in Table 1. The RGs properties are taken from NASA/IPAC Extragalactic Database (NED), except for the 6C objects where the redshifts are taken from Best, Longair & Röttgering (1996), Rawlings, Eales & Lacy (2001) and Inskip et al. (2005), and the 6C* and TOOT objects which are described by Jarvis et al. (2001) and Vardoulaki et al. (2009), respectively. Further details of the RGs will be presented elsewhere (Fernandes et al., in preparation).

2.1 Selection

The quasars were selected by their optical colours in the SDSS Quasar Survey (Schneider et al. 2005). Using the SDSS to select the quasars allowed us to select a large enough initial sample that the RLQ and RQQ samples were chosen in identical ways. The initial sample that met the SDSS colour criteria for quasars was then cross-referenced with the NRAO VLA Sky Survey (NVSS; Condon et al. 1998), the Very Large Array (VLA) Faint Images

Table 1. The RGs used in this paper. Column 2 gives the observed-frame 325 MHz flux density, column 3 the spectral index and column 4 the redshift. The 325 MHz flux densities and spectral indices ($S_\nu \propto \nu^{-\alpha}$) are calculated by fitting a power law through available flux density measurements taken from the NED, except for 6C* and TOOT objects which are not listed in NED, see text for details. The errors associated with the flux densities are typically a few per cent.

Name	S_{325} (Jy)	α	z
3C 175.1	6.939	0.85	0.920
3C 184	9.097	0.87	0.994
3C 22	8.348	0.90	0.936
3C 268.1	15.615	0.58	0.970
3C 280	16.025	0.81	0.996
3C 289	8.278	0.84	0.967
3C 343	13.413	0.68	0.988
3C 356	6.820	1.04	1.079
6CE0943+3958	1.182	0.85	1.035
6CE1011+3632	1.190	0.79	1.042
6CE1017+3712	1.540	1.00	1.053
6CE1019+3924	1.690	0.94	0.923
6CE1129+3710	1.543	0.89	1.060
6CE1212+3805	1.408	1.06	0.95
6CE1217+3645	1.402	0.94	1.088
6CE1256+3648	1.760	0.81	1.07
6CE1257+3633	1.036	1.08	1.004
6C* 0128+394	1.322	0.50	0.929
6C* 0133+486	0.742	1.22	1.029
5C 6.24	0.839	0.77	1.073
5C 7.17	0.469	0.93	0.936
5C 7.23	0.546	0.78	1.098
5C 7.242	0.304	0.94	0.992
5C 7.82	0.371	0.93	0.918
TOOT 1066	0.098	0.87	0.926
TOOT 1140	0.298	0.75	0.911
TOOT 1267	0.282	0.80	0.968

of the Radio Sky at Twenty-cm (FIRST) survey (Becker, White & Helfand 1995) and the Westerbork Northern Sky Survey (WENSS; Rengelink et al. 1997) to pick out the RLQs and RQQs.

RLQs were chosen to have a low-frequency WENSS (325 MHz) flux density of greater than 18 mJy which is the 5σ limit of the survey. At $z \sim 1$ this corresponds to a radio luminosity almost entirely within the radio-loud domain. Fig. 2 compares our sample to an alternative definition of radio loudness used by Ivezić et al. (2002). Here radio-loud objects are defined to have $R_i > 1$ where $R_i = \log(F_{\text{radio}}/F_i)$ and F_{radio} and F_i are flux densities measured at 1.4 GHz and in the i band, respectively (K -corrections are not applied). With the exception of four objects, all of our RLQs would be considered radio loud using this definition. We note that these four objects have only one flux density measurement at radio wavelengths, and hence may in fact fall above the line if their spectral indices differ from the value we have assigned to them, i.e. 0.7 which is the mean value of the measured spectral indices. Using a low-frequency radio flux to define the RLQs allows them to be compared more easily to the RGs without a severe orientation bias.

The RQQs were defined as being undetected by the FIRST survey at the 5σ level. FIRST was used for this definition because it provides a more sensitive flux density limit than WENSS. In this case, the RQQs are not selected to be true radio-quiet objects as defined by the radio-loudness parameter for example. In order to get an estimate for the average radio power of the RQQs in our

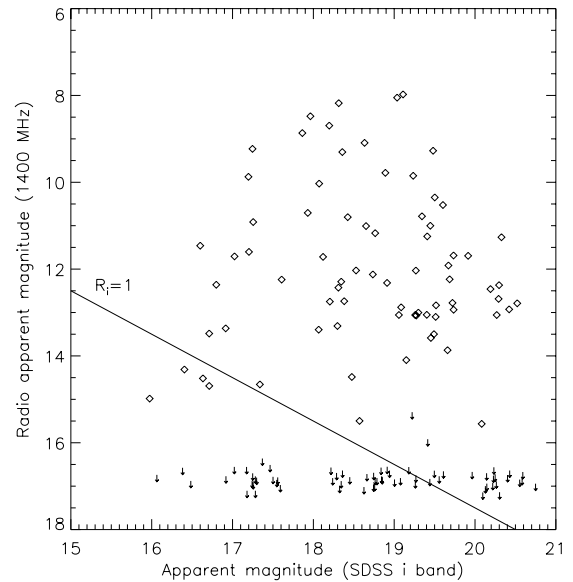


Figure 2. Optical apparent magnitude (SDSS i band) versus radio apparent magnitude (NVSS 1400 MHz) for the quasar samples. RLQs are plotted as diamonds while RQQs are shown as upper limits. The line shows the parameter $R_i = 1$ (Ivezić et al. 2002) which is used to determine radio loudness, i.e. objects falling above the line are classified as radio loud while objects falling below the line are classified as radio quiet. The plot shows that, by this definition, all but four of our RLQs would be classified as radio loud and that at least two-thirds of our RQQs would be classified as radio quiet.

sample we have used a technique of stacking the radio images of non-detections to reveal the average value of the FIRST radio power (e.g. White et al. 2007). In essence it involves stacking up the radio images at the known positions of the RQQs, weighting each image by its standard deviation and then computing the average radio emission or obtaining a sensitive upper limit. The stacked image is shown in Fig. 3. Using this technique we find an average flux density for our RQQs at 1.4 GHz of 0.10 ± 0.02 mJy (i.e. a 5σ detection). Assuming a spectral index of 0.7 allows us to extrapolate to a 325-MHz flux density of 0.30 ± 0.06 mJy which at $z \sim 1$ corresponds to a 325-MHz luminosity, $\log_{10}(L_{325}/\text{W Hz}^{-1} \text{sr}^{-1}) = 23.02$.

Lists of around 75 RLQs and 71 RQQs were chosen for observation to be matched in optical luminosity and span the full 5 optical magnitudes available; the selected sources are shown in bold in Fig. 1. The distribution of optical magnitudes within the selected redshift range is shown in Fig. 4. The RGs were selected from the low-frequency (178 or 151 MHz; orientation independent) radio samples 3CRR (Laing, Riley & Longair 1983), 6CE (Eales 1985), 7CRS (Willott et al. 1988) and TOOT surveys (Hill & Rawlings 2003). Together, these surveys give 27 RGs in the same $0.9 < z < 1.1$ redshift range as our quasars. The reason therefore for our substantially smaller RG sample is purely due to the limit of the known RG population at $z \sim 1$.

The RLQ and RG radio luminosity distribution within the selected redshift range is shown in Fig. 5 which shows that, on average, the RGs are more radio luminous than the RLQs, albeit with a significant overlap. Using the FIRST radio images we can also place an upper limit on the radio emission of each RQQ; see Figs 2 and 5, which shows that at least two-thirds of our RQQs and most likely more would be classified as radio quiet using the definition from

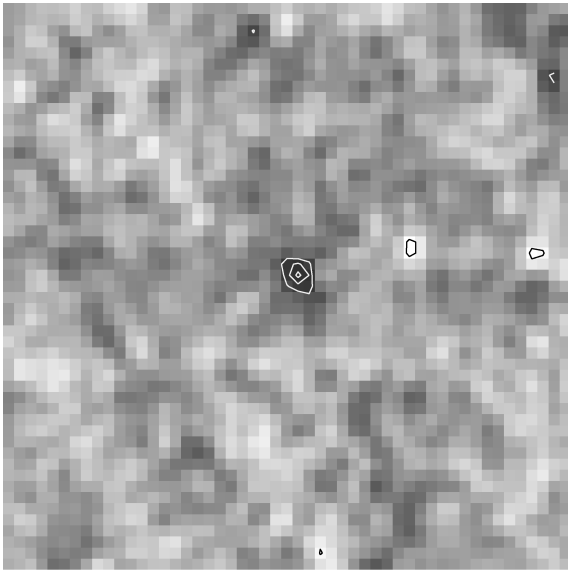


Figure 3. Stacked and averaged radio image of the positions of our RQQs using data from the FIRST survey. The contours show the 3-, 4- and 5σ levels. Black contours are negative and white are positive. The image dimensions are 1.5×1.5 arcmin².

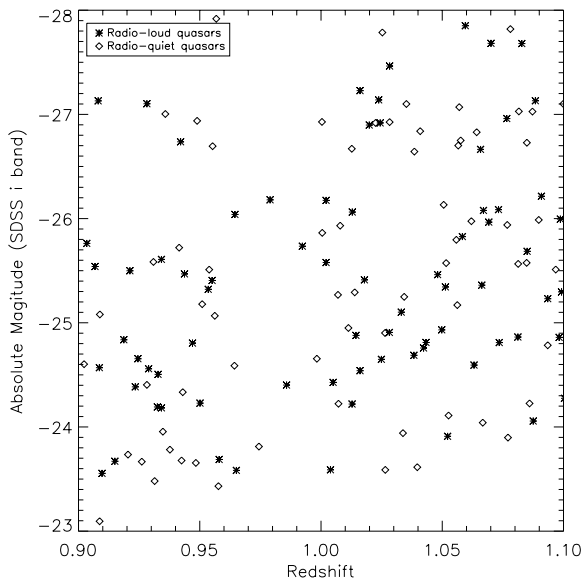


Figure 4. Optical absolute magnitude (SDSS *i* band) versus redshift for the quasars. RLQs are shown with asterisks and RQQs with diamonds.

Ivezić et al. (2002). In comparison to these limits the least radio-loud RLQ has a 325-MHz luminosity of $\log_{10}(L_{325}/W \text{ Hz}^{-1} \text{ sr}^{-1}) = 24.5$, showing that there is at least an order of magnitude difference (several between the means) in the radio emission of our RQQs and RLQs. The reason for the gap between the RLQs and RQQs in radio luminosity seen in Fig. 5 is due to the difference in the survey depths of the WENSS and FIRST surveys from which they were selected. The 5σ limit used for the RLQ lower limit and the RQQs upper limit are not identical, as shown by the dashed and dotted lines in Fig. 5. This leaves a small region on the radio luminosity axis uncovered by our data, but it is important to note this is due to our selection rather than evidence for a real radio power dichotomy.

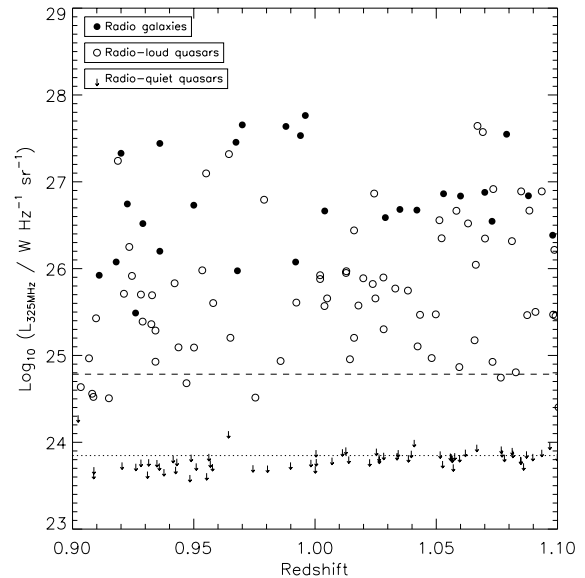


Figure 5. Low-frequency radio luminosity versus redshift for our sample. RLQs are shown with open circles and RGs with filled circles (data are rest-frame 325 MHz from WENSS). For the RQQs, 5σ upper limits (extrapolated to rest-frame 325 MHz) from the FIRST survey are shown. Where WENSS data were unavailable for the RLQs due to sky coverage (about 10 objects) the 325-MHz flux density was extrapolated from the NVSS survey at 1400 MHz assuming $\alpha = 0.7$. The dashed line shows the average 5σ limit of the WENSS survey, converted to a luminosity at $z = 1$ by assuming $\alpha = 0.7$; the RLQs were selected to have radio luminosities falling above this line. The dotted line shows the average 5σ limit of the FIRST survey, extrapolated to 325 MHz and again converted to a luminosity; the RQQs were selected to have a radio luminosity falling below this line. The assumed spectral indices for some conversions explain why some objects fall between the lines on this plot.

2.2 Observations and data reduction

We omitted from our *Spitzer* observations all targets which lie within the overlap regions of the SDSS, the *Spitzer* Wide-Area Infrared Extragalactic Legacy Survey (SWIRE; Lonsdale et al. 2003) and the Extragalactic First Look Survey (XFLS; Lacy et al. 2005) regions. This was because Richards et al. (2006) has already compiled the data for these objects, of which two are RLQs and 15 are RQQs. We also found that two of the 3C RGs have adequate data in the archive: 3C 356 (ID3329; PI Stern) and 3C 184 (ID17; PI Fazio). These data were downloaded from the *Spitzer* archive and added to our own observations which are described below.

Our IRAC observations were carried out in all four bands between 2006 August and 2007 August. We performed 5-point Gaussian dithers with the medium cycling pattern and 12 s frame time to ensure good scattered light rejection and good photometry. The data were reduced with the standard pipeline version S15.0.5 giving final maps with a pixel scale of 1.2 arcsec. In this paper we use the 3.6- μm channel to study the environments of our AGN since it samples light emitted at $1.8 \mu\text{m}$ at $z \sim 1$ which is close to the peak of the stellar emission from galaxies. It is also the most sensitive IRAC channel. An aperture correction of 1.48 was applied to the 3.6 μm flux densities, as determined by the *Spitzer* First Look Survey (Lacy et al. 2005). Full details of the observations and data reduction are given in Jarvis et al. (in preparation).

3 SOURCE EXTRACTION

The images were cut down using IRAF tasks to leave $3.4 \times 3.4 \text{ arcmin}^2$ images centred on the position of the AGN. This process removes any edge effects and underexposed edges caused by the dither pattern, but leaves enough area to sample the AGN environment out to a radius of 800 kpc at $z \sim 1$. To create catalogues of the images we used the SExtractor software package (Bertin & Arnouts 1996). We used a detection threshold of 3 adjacent pixels each at 1.5σ above the rms background level. The SEEING_FWHM was set to 1.67 arcsec which is the measured resolution of our images. On inspection of the output catalogues it was found that the default value for the deblending parameter (0.005) resulted in non-detection of faint sources close to bright AGN and stars. We therefore adopted the value used by Lacy et al. (2005) of 0.0001 which gave a significant improvement, although in a small number of cases it led to the inclusion of spurious sources identified with diffraction spikes.

To check for spurious sources we inverted the maps and ran the same source extraction configuration. The results showed that 96 per cent of the fields had no spurious 5σ sources. However, the remaining 4 per cent had spurious sources associated with the diffraction spikes of bright stars (which give pronounced negative artefacts). We therefore used this method to identify those images affected by diffraction spikes and then manually checked their non-inverted catalogues for sources that were obviously spurious, these were then removed from the catalogues.

3.1 Source cuts

The catalogues were filtered to reduce the noise produced by spurious and foreground sources. Filtering criteria were applied identically to the AGN fields and the blank fields (see below).

In order to ensure that all images were of the same sensitivity a cut was made of source detections below a conservative 5σ level (see Fig. 6). This level is defined as the 5σ level of the shallowest

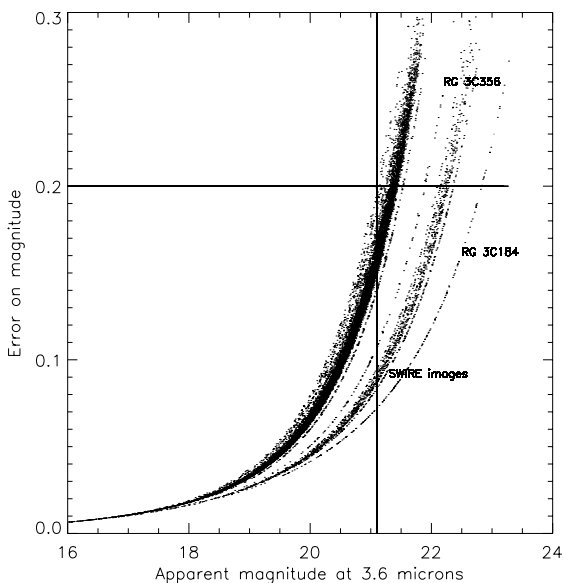


Figure 6. The apparent magnitudes of all sources at $3.6 \mu\text{m}$ versus the error on that magnitude. The deeper SWIRE images are labelled, and the lines show the 0.2 mag error (5σ) level and the corresponding magnitude for the shallowest image, i.e. 21.1 mag . The two other smaller bands shown and labelled are from the two RGs which had already been imaged by other programmes; see the text for details.

image in the sample thus ensuring that any sources used could be detected in any image. The cut is especially necessary because of the use of images from SWIRE and the archive which are deeper than our own. Using this method, all sources in our fields with apparent magnitudes fainter than 21.1 ($13.1 \mu\text{Jy}$) were excluded from our analysis. To put this limit into context, the absolute magnitude of the break in the K -band galaxy luminosity function at $z \sim 1$ is $K^* = -23.0$ (Cirasuolo et al. 2010). An elliptical galaxy at $z \sim 1$ has $K - 3.6 = 0.27$ (Bruzual & Charlot 2003) giving an equivalent break in the $3.6 \mu\text{m}$ luminosity function of -23.3 or an apparent magnitude of $m_{3.6}^* \sim 20.8$. Thus at the 5σ depth of our survey we are sensitive to galaxies with $3.6 \mu\text{m}$ luminosities of $\sim L^*$ or greater. We are sampling starlight emitted longwards of the Balmer break at $z \sim 1$ so any companions to the AGN are likely to be galaxies with a substantial old stellar population.

In order to remove stars the SExtractor CLASS_STAR output parameter was used. This returns a value between 1 and 0 where 1 is a perfectly star-like object and 0 is very non-star like. We have cut all sources that have a CLASS_STAR parameter greater than 0.8, as used by Best et al. (2003) and Smith, Boyle & Maddox (2000). We also ran the same analysis using 0.95, another commonly adopted value, and found almost identical results, suggesting that most objects cut at the 0.8 level had values greater than 0.95.

4 ANALYSIS

Once the catalogues were created they were searched for sources in annuli working out from the target AGN. The annuli were kept to a fixed area, rather than fixed width; this keeps the signal-to-noise ratio and Poisson errors of similar size from bin to bin and also allows for a larger number of annuli. The target AGN is excluded from the galaxy counts as this would bias the results towards there being an overdensity in the first bin.

To get an estimate for the average number of counts in the field to compare with the AGN fields, we have made use of the extra adjacent field that comes with *Spitzer* images. This is a result of the way *Spitzer* works. IRAC has four detectors but can only point two at the target at any one time so the telescope has to offset to allow the other two detectors to image the target. While this happens the untargeted detectors image a region of an adjacent field to the same depth as the target fields. As these fields are not targeted at the AGN they can be used as blank or control fields, and were thus treated in exactly the same way as the AGN fields. Hence the region with the same exposure time as the main fields was source extracted in the same manner as the AGN fields and the average source density was computed.

We can also use the blank fields to get a measure of the local foreground and background in each region and subtract the mean source density in each blank field from its AGN field. In this case, we are measuring the source overdensity rather than just the source density, which better allows us to stack the results. One possible pitfall of this approach is that the blank fields might be close enough to the AGN that any overdensity will extend into them. The proximity of blank fields to the target fields is therefore a trade-off between the desire to subtract a local foreground whilst not wanting to be so close that any overdensity is also subtracted.

For comparison we have calculated the global source density level for the SWIRE fields using the same source cuts described above. Our background source density is $7.34 \pm 0.35 \text{ arcmin}^{-2}$ which compares to the overall SWIRE average from the three northern fields (covering $\sim 25 \text{ deg}^2$) of $6.79 \pm 0.34 \text{ arcmin}^{-2}$. The quoted uncertainties in these backgrounds are calculated by adding the Poisson

and cosmic variance errors in quadrature. Cosmic variance errors were calculated by placing 173 tiles on to the SWIRE fields, each having an equal area to one of our blank fields to give a mock survey of equivalent area to that of our real survey. We repeated this procedure 43 times and calculated the mean background level and its standard deviation which is the cosmic variance error. At face value, our fields have a slightly higher average background level than the SWIRE fields but they are entirely consistent within the errors.

Does this analysis imply that any overdensity surrounding our AGN extends into the blank fields? This is unlikely for the following reasons. First, there is evidence in the literature that overdensities for the most powerful RGs (at $z \sim 1.6$) extend out to, at most, 1.6 Mpc (Best et al. 2003) whereas our blank fields are at their closest point ~ 2.8 Mpc (at $z \sim 1$) from the AGN. Secondly, when we break the blank fields into strips we see no increase in source density towards the AGN. It is possible that the increased background could be due to stars that are not removed by the `CLASS_STAR` parameter cut. This may be a larger effect in our images since the SWIRE fields are confined to high Galactic latitudes which are often pre-selected to have low foregrounds whereas our fields are more evenly spread over the northern SDSS regions.

4.1 Completeness

In order to measure and correct for the completeness of our data we conducted extensive simulations to add and recover artificial sources. We added 1000 sources in to each of our AGN fields for 30 flux bins (i.e. 30 000 sources per image) and proportionally less for the blank fields as they are of a smaller area. These sources were chosen to be Gaussian with a full width at half-maximum (FWHM) of 2 arcsec, and were scaled to the required flux. They were added across each image in a grid pattern in batches of 100 for the AGN fields and proportionally less for the blank fields. The sources were allowed to randomly move around within the grid as far as possible without two sources ever being placed close enough as to not be deblended. Sources were considered to be recovered if they were found in the `SExtractor` catalogues within 1.5 pixels (1.8 arcsec) of their input position and had an extracted flux within a factor of 2 of the input value. In the AGN fields we computed the completeness for each annulus individually which allows us to correct for bright objects masking regions of certain annuli. In the blank fields we used the average completeness for the whole blank field region as we are only interested in attaining one value per field.

To eliminate the scatter in the measured completeness curves we then fitted them with an empirical model of the form $\text{completeness} = (S^a)/(b + cS^a)$ (Coppin et al. 2006), where S is the 3.6- μm flux density and a , b and c are constants that are fitted. An example of one of these fits with the overlaid data points is shown in Fig. 7. This process then allowed us to apply a different completeness correction to every annulus in each image as a function of flux which corrects for any lost area due to bright stars or diffraction spikes as well as sources lost due to being in crowded regions.

As expected, the completeness is lower than average in the first annulus of the quasar fields which is due to the bright AGN hindering the detection of faint sources (see Fig. 8). This effect was also noted by Yee & Green (1984). Indeed, we find a highly significant correlation between the optical magnitude of the AGN and the completeness of the first bin for the quasars at the 99.7 per cent level using correlation analysis (Spearman rank and Kendall tau). Hence applying the completeness corrections was found to boost the source density in the first annulus relative to the others (although

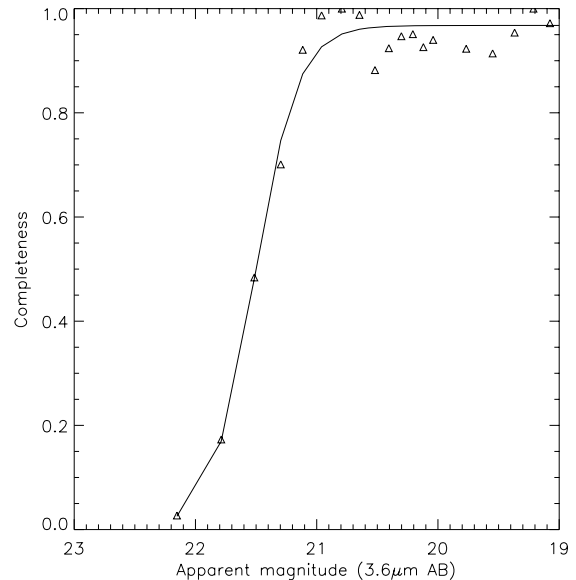


Figure 7. An example of a completeness curve with empirical model fit. Our flux limit is $13 \mu\text{Jy}$ which is therefore the lowest flux at which we use a completeness correction.

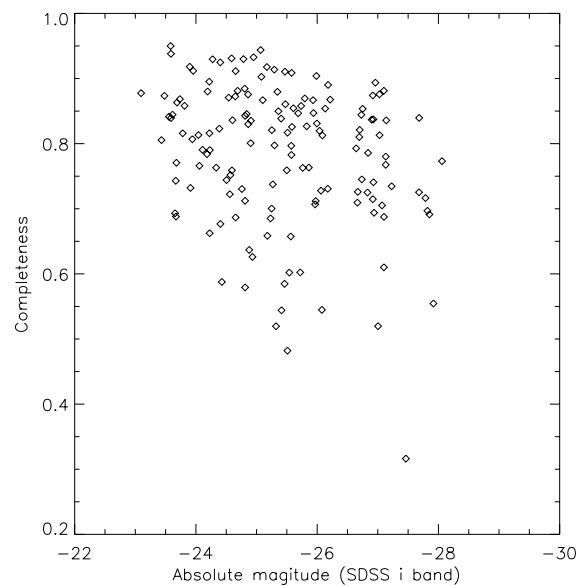


Figure 8. Plot showing the optical absolute magnitude (SDSS i band) versus the completeness at our flux limit ($13 \mu\text{Jy}$) in the first annulus for all the quasars in our sample. Correlation analysis shows a correlation at the 99.7 per cent level.

the significance is not changed as the error is also scaled by the completeness). This effect is not as prominent in the RG fields as they are generally less luminous in the optical/infrared, due to the quasar nucleus being obscured so that we only see the stellar light from the host galaxy.

5 RESULTS

Conducting the radial search on individual fields does not give significant results because the IRAC data are dominated by foreground sources. There are also large Poisson errors resulting from counting small numbers of objects. However, these problems are reduced if

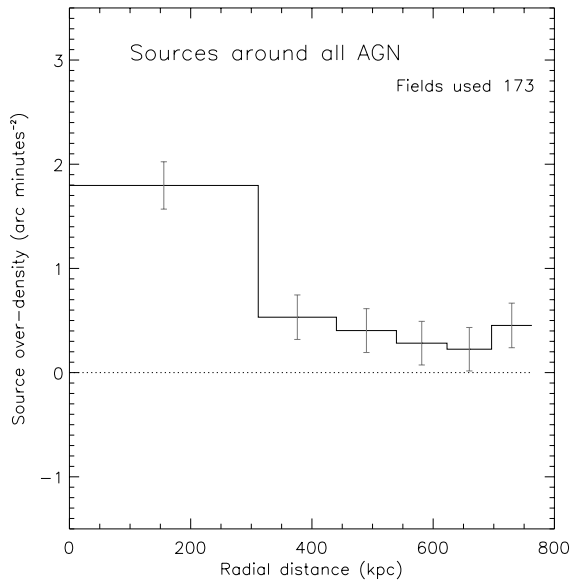


Figure 9. Histogram showing the average source overdensity in all the AGN fields after they were corrected for completeness and the local background has been subtracted. The error bars for each field are the Poisson error for each bin combined in quadrature with the Poisson error on the blank field level that was subtracted, both scaled by their mean completeness correction; these values are then added in quadrature to give the final error bar on the stacked histogram. The dotted line simply highlights the zero level.

multiple fields are stacked up because the larger number of counts involved reduces the associated Poisson errors, as well as averaging out the variations in foreground sources. Hence in this paper we concentrate mainly on a statistical analysis of stacked data from multiple fields.

5.1 Overdensity for the whole AGN sample

In Fig. 9 we show the results of a radial search conducted on all our AGN fields, centred on the AGN, stacked together and averaged. Note that the local background level calculated from the blank field of each AGN has been subtracted so the plot shows source overdensity rather than source density. The error bars for each field are the combined Poisson errors of the count in the AGN field added in quadrature to the Poisson error of the blank field value that was subtracted, both scaled by their mean completeness correction; these are then added in quadrature to give the final error bar on the stacked histogram. It is obvious that there is an overdensity in the AGN fields as a whole, since all of the bins have a nominal value above the background level, but also a big increase in this excess towards the position of the AGN.

It thus appears that the bulk of the overdensity is concentrated within the first bin or within 300 kpc (physical units) of the target AGN. The chosen bin size came from a trade-off between gaining a reasonable signal-to-noise ratio in the first bin whilst not watering down the overdensity by including too large an area. The radial search was thus repeated using annuli of varying size and it was found that the optimum size is that adopted, which has an area of 1.4 arcmin^2 . This exercise also showed that, even when smaller bins were used, the central overdensity still extended to 200–300 kpc before dropping towards the background level.

To calculate the significance of the overdensity in each bin, we simply use the number of 1σ error bars that the overdensity is above zero. This is shown in Table 2 which shows the relevant values for

Table 2. The overdensity shown in Fig. 9 tabulated for each bin and as an average for the outer bins (i.e. excluding bin one). The table shows the overdensity (ΔN), the overdensity error ($\text{err } \Delta N$) and the σ value which is the number of 1σ error bars ($\text{err } \Delta N$) that the overdensity (ΔN) is above zero.

Bin	ΔN (arcmin^{-2})	$\text{err } \Delta N$ (arcmin^{-2})	σ
1	1.80	0.21	8.50
2	0.53	0.20	2.71
3	0.40	0.19	2.08
4	0.28	0.19	1.46
5	0.22	0.19	1.17
6	0.45	0.20	2.29
Outer bins	0.38	0.09	4.26

each annular bin of the histogram shown in Fig. 9. It can be seen that if we just consider the first bin this is overdense at the 8.5σ level.

In order to test whether the overdensity in the outer bins (excluding bin one) is significant we added the counts in the outer bins and calculated the combined Poisson error. This gives an overdensity of $0.37 \pm 0.09 \text{ arcmin}^{-2}$ and a significance of 4.3σ (see Table 2). Therefore, the outer bins are also significantly overdense (out to at least 800 kpc) but the bulk of the overdensity is mainly found in the first bin. This pattern of a sharp peak in the central source overdensity and then an extended flatter overdensity was also reported by Best et al. (2003) for powerful RGs at $z \sim 1.6$, and by Serber et al. (2006) for $M_i \leq -22$, $z \leq 0.4$ SDSS quasars.

5.2 Overdensity versus AGN type

To investigate trends with AGN classification we have divided the AGN into RQQ, RLQ and RG subtypes and performed a similar analysis to that described in Section 5.1. The results of this analysis are shown in Fig. 10. On first inspection, the most notable difference between the subsets is the apparently larger overdensity in the RLQ and RG samples when compared to the RQQ sample.

Using the same method as for the whole sample described in Section 5.1, we have calculated the significance of the overdensity in each annulus for each of these subsamples. The main results are summarized in Table 3 which shows the overdensities in the first three bins and their significances and the same values in just the outer bins (excluding bin one). Focusing on the first bin, which in all cases appears to contain the bulk of the overdensity, we find overdensities for the RGs of 4.0σ , for the RLQs of 5.9σ and for the RQQs of 3.7σ . The lower significance level for the RG sample probably just reflects the small sample size. It is worth noting that in this subset the second bin is also significant at the 2.8σ level, which if combined with the first bin would give a more significant overdensity.

To quantify the difference we see in the first bins of the RLQs and RQQs we conducted a Mann–Whitney test, which is a non-parametric form of a t -test, and gives the probability that two data sets, in our case the source overdensities around our AGN, have the same mean. Considering source densities in the first bin this test indicates that the RLQs inhabit, on average, more dense environments than the RQQs at the >96 per cent confidence level. It therefore appears that all of our AGN have a significant overdensity out to ~ 300 kpc with the radio-loud objects, on average, having larger overdensities. Interestingly the RGs appear to have a larger

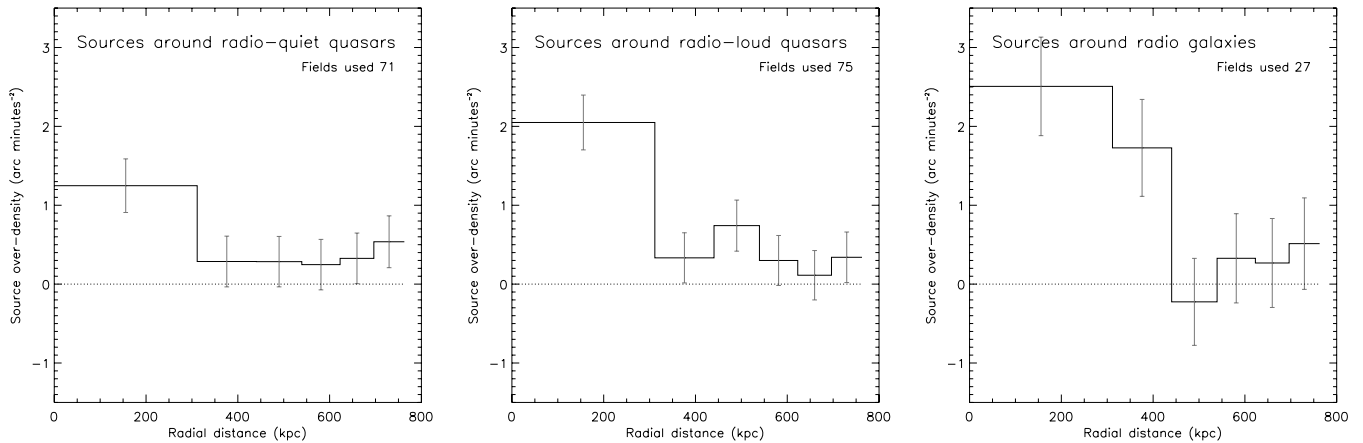


Figure 10. Histograms showing the averaged source overdensity for the AGN subsamples. The right-hand panel shows the RQs, the middle panel shows the RLQs and the left-hand panel shows the RGs. The error bars for each field are the Poisson errors for each bin combined in quadrature with the Poisson error on the blank field level, that was subtracted, both scaled by their mean completeness correction; these values are then added in quadrature to give the final error bar on the stacked histogram. The dotted lines simply show the zero levels.

Table 3. The overdensities from Fig. 10 shown for the first three bins and as an average for the outer bins (excluding bin 1). The table shows the overdensity (ΔN) and the sigma value which is the number of 1σ errors that the source density is above the blank field source density.

AGN type	Bin	ΔN (arcmin ⁻²)	σ
Radio galaxies	1	2.51	4.01
	2	1.73	2.81
	3	-0.22	-0.41
	Outer bins	0.52	2.15
Radio-loud quasars	1	2.05	5.90
	2	0.33	1.05
	3	0.74	2.29
	Outer bins	0.37	2.73
Radio-quiet quasars	1	1.25	3.67
	2	0.29	0.89
	3	0.28	0.89
	Outer bins	0.34	2.48

central overdensity than in the quasar fields although more RG data are needed to confirm this tentative result.

In order to test that these results are not being caused by the presence of a few very overdense fields which happen to fall into our radio-loud samples we removed the five most overdense fields from our RLQs and the five least overdense fields from our RQs. The observed trend for the first bin still holds, although obviously there is a drop in significance due to removal of the most extreme fields in each case. It is clear from this analysis, however, that there is a fair amount of field-to-field variation which could be attributed to either actual changes in the environmental richness between fields or to field-to-field changes in the foreground/background contamination.

5.3 Black hole mass versus environmental density

In order to try to understand the contrast between the fields of the radio-loud and radio-quiet objects we can use estimates of black hole mass to search for possible trends. For example, are the biggest

overdensities found around the AGN which host the largest black holes?

Our black hole mass estimates are computed using the virial estimator and the Mg II line at 2800 Å using SDSS spectroscopy, a technique described by McLure & Jarvis (2002), and based on work by McLure & Dunlop (2004). Note that we do not have black hole mass estimates for the RGs because the broad-line region is obscured in these objects, but estimates are available for all of the quasars.

To test whether the difference we find between the fields of the RLQs and RQs might be related to intrinsically different black hole mass distributions, as suggested in previous papers (e.g. Lacy et al. 2001; McLure & Jarvis 2004), we again conducted a Mann-Whitney test. The test suggested that the mean black hole masses for the two samples are not significantly different; the returned probability that they have the same mean is 0.32. Moreover, a two-sample Kolmogorov-Smirnov (K-S) test returns a probability of 0.90 that the samples are drawn from the same parent distribution. We stress that this result does not contradict previous work but is rather a direct consequence of the manner in which our samples were initially matched in absolute optical magnitude and colours as well as the relatively small sample size. The mean black hole masses are ($\log_{10}(M_{\text{BH}}/M_{\odot}) = 8.87 \pm 0.06$ for the RLQs and ($\log_{10}(M_{\text{BH}}/M_{\odot}) = 8.81 \pm 0.06$ for the RQ so the means of the two samples are consistent and well within 1σ of each other. In any case the real uncertainties are likely to be bigger once systematics are taken into account. The distribution of black hole masses is shown for both samples in Fig. 11.

We can go one step further by testing whether overdensity is related to black hole mass regardless of AGN classification. This is shown in the left-hand panel of Fig. 12. To search for possible trends we performed a correlation analysis on the AGN overdensity measurements in the first bin. We have used two types of correlation analysis: the Spearman rank order test and the generalized Kendall's tau test. Both tests suggest a low probability of a correlation (see Table 4).

A possible source of uncertainty in the black hole masses of RQs and RLQs could be their orientations with respect to the observer. As shown by Jarvis & McLure (2002) and Jarvis & McLure (2006) one would expect that sources with bright core radio emission would be preferentially aligned pole-on to the observer. Coupled with

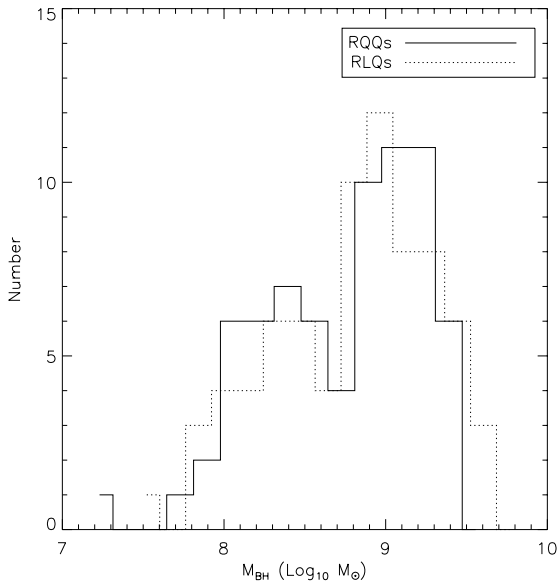


Figure 11. Histograms showing the distributions of RLQ and RQQ black hole mass estimates.

a disc-like broad-line region, such a bias would result in lower derived black hole masses for the RLQs relative to the RQQs given the same optical selection. However, our initial selection, based on low-frequency radio emission using the WENSS at 325 MHz, means that we minimize beaming effects as the radio emission at low frequencies is dominated by the extended, optically thin, lobe emission. Therefore, although we cannot rule out completely a link between environmental density and black-hole mass for our sample, it would seem very unlikely.

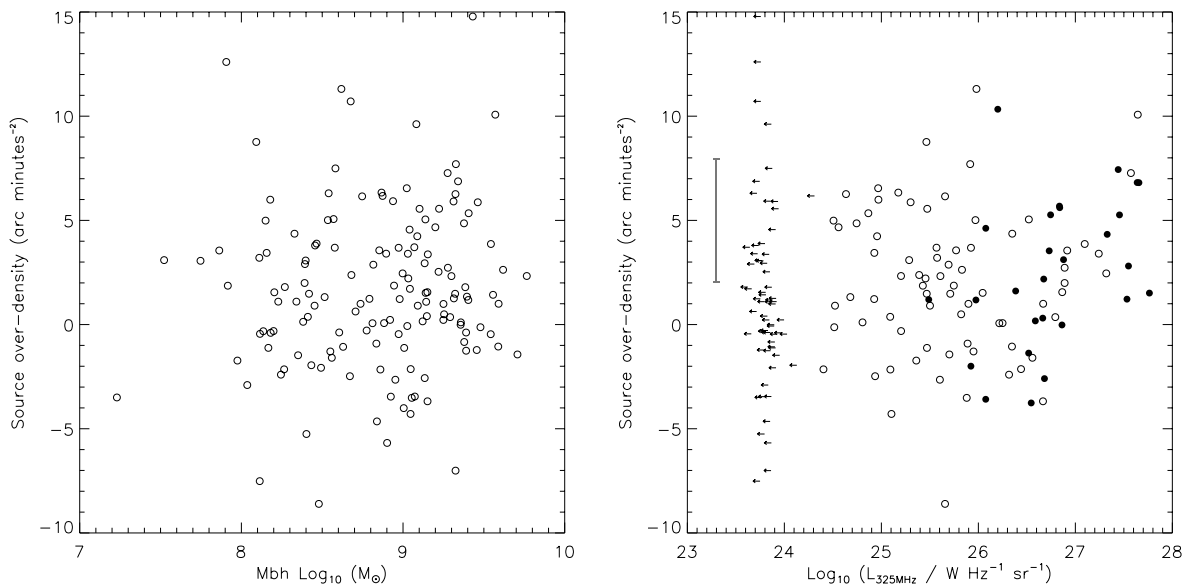


Figure 12. Source density within ~ 300 kpc at $z \sim 1$ as a function of black hole mass for the quasars (left-hand panel) and as a function of radio luminosity at 325 MHz for all AGN (right-hand panel). In the right-hand panel, the open circles show the RLQs, the filled circles the RGs and the upper limits the RQQs; also shown in this panel is an example of the size of the error bars on the overdensities in both panels. The error bars would show the Poisson error for each AGN field combined in quadrature with the Poisson error on the blank field level, that was subtracted, both scaled by their mean completeness correction.

5.4 Radio luminosity versus environmental density

Having upper limits for the RQQ radio power (see Section 2.1) allows us to investigate the environmental densities of all our AGN as a function of radio luminosity (see Fig. 12). Since the RGs are not selected in the same way as the quasars, caution must be exercised in their inclusion in this analysis. It is also worth noting the size of the error bars on the overdensity in these figures, as shown by the mean error bar ($\pm 3 \text{ arcmin}^{-2}$). This explains the large scatter on any correlation.

The censored data (e.g. the RQQ upper limits) require that we use survival analysis techniques for our correlation analysis. We therefore used IRAF which provides three types of test: the Spearman rank order test, the generalized Kendall's tau test and the Cox proportional hazard model. All three tests can handle one type of limit in the dependent variable, in our case upper limits in the radio luminosity. The results of the correlation analysis are shown in Table 4. With the exception of the Cox proportional hazard model the tests give evidence for a correlation at the >95 per cent confidence level when all AGN are included. We also restrict our analysis to those sources that have radio luminosities above the traditional separation between Fanaroff–Riley I (FRI) and Fanaroff–Riley II (FR II) radio sources at $\log_{10}(L_{325}/W \text{ Hz}^{-1} \text{ sr}^{-1}) = 25$ (see e.g. Clewley & Jarvis 2004). At this threshold there is also a divergence in the space-density evolution with redshift, with the higher luminosity radio sources tending to evolve more strongly than the lower luminosity sources (Clewley & Jarvis 2004; Sadler et al. 2007). For this sample we again obtain correlation at the >95 per cent level. However, if we employ a much more conservative low-luminosity cut-off of $\log_{10}(L_{325}/W \text{ Hz}^{-1} \text{ sr}^{-1}) = 26$ which ensures that all of our sources lie well within the FR II regime then we find that the correlation is significant at the >99 per cent level.

Intriguingly, in the high radio luminosity range the RLQs and RGs appear to show the same trend of increasing source overdensity with radio luminosity, as would be expected in the unified scheme (Barthel 1989). This improvement in the correlation analysis results

Table 4. Correlation analysis on the data from Fig. 12, i.e. source density within ~ 300 kpc at $z \sim 1$ versus black hole mass for the quasars and then versus radio luminosity for all AGN. AGN ($L_{\text{radio}} > 25$ or 26) corresponds to AGN with $\log_{10}(L_{325}/\text{W Hz}^{-1} \text{sr}^{-1}) > 25$ or 26. Coefficients shown are the correlation coefficient except for the Cox hazard test which gives a χ^2 value. The significance shown is the confidence level at which the null hypothesis (i.e. no correlation) can be rejected. Survival analysis was used on the radio luminosity data as these contain upper limits on the RQs radio luminosity.

	Test	Coefficient	Significance
Quasars (M_{BH} versus overdensity)	Spearman rank	0.080	0.666
	Kendall tau	0.054	0.669
All AGN (radio luminosity versus overdensity)	Spearman rank	0.160	0.961
	Kendall tau	0.215	0.966
	Cox hazard	2.109	0.854
AGN ($L_{\text{radio}} > 25$) (radio luminosity versus overdensity)	Spearman rank	0.226	0.963
	Kendall tau	0.155	0.966
AGN ($L_{\text{radio}} > 26$) (radio luminosity versus overdensity)	Spearman rank	0.483	0.992
	Kendall tau	0.121	0.999

for high radio luminosity could of course be a real effect or instead it might be a result of foreground/background contamination in some of the low radio luminosity AGN causing them to appear more overdense than they actually are. However, recent work by Donoso et al. (2009) finds that the environmental densities of RLQs and radio-loud AGN (i.e. RGs) match only for radio luminosities of $\log_{10}(L_{325}/\text{W Hz}^{-1} \text{sr}^{-1}) \gtrsim 25.4$ (after converting into appropriate units). Their interpretation is that the unified scheme for RLQs and RGs might only be valid for high radio luminosities. Finally, we note with interest that Donoso et al. (2009) also report a similar trend to that found here of increasing environmental density with radio luminosity for RLQs.

6 DISCUSSION

Our results indicate that, on average, AGN at $z \sim 1$ have two to three massive ($\gtrsim L^*$) galaxies containing a substantial evolved stellar population in their ~ 300 -kpc-scale environments, representing an overdensity relative to the field.

Moreover, we find evidence that the radio emission we observe from AGN is in some way related to the galaxy density in its environment. Specifically, we find that the RLQs and RGs occupy more dense environments than the RQs. Secondly, if we ignore AGN classification and simply measure the overdensity as a function of radio luminosity (Fig. 12) we find evidence of a positive correlation between the two (Table 4).

Initially one might expect that these results could be due to the radio-loud objects having intrinsically larger black hole masses than their radio-quiet counterparts. Indeed, recent work has found evidence for this to be the case (e.g. Lacy et al. 2001; McLure & Jarvis 2004). If we then assume that the largest black holes reside in the largest dark matter haloes, or are found closer to the centre of their haloes, they would thus also have the highest density environments. However, when we compare our results to the quasar black hole mass estimates we find that the black hole masses of the RLQs and RQs are statistically indistinguishable. Moreover, the overdensity around the quasars shows no significant trend with black hole mass (Fig. 12) using a correlation analysis (Table 4).

At this point it is worth considering whether there might be a systematic bias in the way our black hole mass estimates are made for the radio-loud and radio-quiet subsets. For example, if the Eddington ratios are for some reason systematically lower for

the radio-loud objects then they must host more massive black holes to produce a given optical luminosity. One possibility is that radio-loud objects are powered by a radiatively inefficient accretion process such as Bondi accretion of the hot phase of the intergalactic medium (IGM; e.g. Hardcastle, Evans & Croston 2007) while the radio-quiet objects are accreting cold gas in the standard manner. However, such a possibility is easily dismissed since radiatively inefficient accretion processes can only explain the multiwavelength properties of low-excitation radio sources which are almost all FRI objects whereas our entire sample is made up of QSOs, with the radio-loud objects all having radio luminosities typical of FRII sources (Fig. 5). Furthermore, given that our samples are matched in absolute optical magnitude and optical colours, any difference in accretion properties must contrive to produce a distribution of Mg II linewidths that would lead to identical black hole mass distributions; this seems unlikely.

Therefore we are led to conclude that the environments of the AGN are somehow affecting the differences we observe in their radio properties. This is one of two possible scenarios that could explain our results, the other being that the AGN radio emission is influencing the environmental density. However, this is a much harder scenario to envisage as the ~ 100 -kpc-scale radio jets would need to influence galaxy formation on Mpc scales.

It is known that tidal stripping would be more prevalent in denser environments, as more close encounters or mergers with other galaxies would occur. The IGM would therefore be denser in regions of higher galaxy density. A higher IGM density gives more material for radio jets to work on, increasing the radio luminosity produced through synchrotron losses. This effect, known as jet confinement, was discussed by Barthel & Arnaud (1996) who use it to explain the unusually steep far-infrared to radio spectral slope of Cygnus A as boosting of the radio luminosity caused by a higher environmental density. The estimated enhancement in radio luminosity for AGN in clusters, compared to the field, was given by Barthel & Arnaud (1996) as ~ 1.5 orders of magnitude which might be sufficient to explain our results, although a realistic physical model is clearly required. In the local universe, Kauffmann et al. (2008) find a similar difference in matched samples of radio-loud and radio-quiet emission line AGN from SDSS; they also offer an explanation in terms of radio jets being enhanced in denser environments. Our results extend this relationship to higher luminosity objects at higher redshifts.

The idea of jet confinement may be able to explain the results for the RGs and RLQs. Whether this idea can be extended to the RQQs, which typically have radio emission at least an order of magnitude lower than the RLQs, is less clear. Classically in unified schemes, RQQs are thought of as the quasars without kpc-scale radio jets, implying that they are physically different to RLQs. However, there is some evidence in the literature to suggest that the radio properties of RQQs and RLQs are not so very different (see Lacy et al. 2001 for example). It has been suggested though, that the use of the FIRST survey, which is not sensitive to extended radio emission, may in fact have been responsible for these findings (Ivezić et al. 2002). However, Kukulka et al. (1998) detect kpc-scale radio jets around 34 per cent of a sample of 27 RQQs. If this is representative of the whole RQQ population then perhaps the classical view is no longer valid and there is in fact more of a continuum of quasar radio properties. This certainly makes the source of the radio emission from AGN easier to understand, as explaining a dichotomy in their properties is difficult. In our sample, there is definitely a gap in the radio luminosities of our quasars (see Fig. 5) in the sense that the RQQ upper limits are typically an order of magnitude below the least RLQs. This effect is, however, intrinsic to our sample, since we have used different surveys which have different depths to define the RLQ and RQQ subsamples. Therefore this is not suggestive of a radio power dichotomy in the quasar population although at the same time it is not evidence that there is not one.

An alternative explanation is that the differences we observe in AGN radio properties are caused by the spin states of their black holes. This is certainly plausible as it could much more readily explain a radio power dichotomy, if indeed it turns out that there is one. It could also explain our results if for some reason the spin is affected by the environmental density. This idea is mentioned in the literature and usually takes the form of black holes spinning faster in dense environments due to increased exposure to mergers, which spin up the black hole (e.g. Wilson & Colbert 1995; Moderski, Sikora & Lasota 1998; Sikora, Stawarz & Lasota 2007; Volonteri, Sikora & Lasota 2007). However, the one major problem with black hole spin as an explanation is that it is as yet not observationally measurable in AGN and so the hypothesis is not yet testable.

7 CONCLUSIONS

We have conducted an analysis of the environments of a large sample of AGN at $z \sim 1$ in order to study the relationship between AGN activity and environmental density at an epoch close to the peak in AGN activity. Our main conclusions are as follows.

(i) The AGN fields show, on average, an excess above the field of two to three massive galaxies containing a substantial evolved stellar population. Most of this overdensity is confined within a radius of 200–300 kpc of the AGN although there is good evidence for a lower level overdensity extending out to the Mpc-scale.

(ii) We find evidence for a trend of increasing galaxy overdensity with increasing AGN radio luminosity. Since the RLQs and RQQs have indistinguishable black hole mass distributions the observed difference in environmental density is not a result of observing different populations of objects. This leads us to conclude that the radio power of an AGN is in some way influenced by the environmental density in which it resides.

(iii) Our results could be explained by the boosting of radio jets in areas of higher IGM density which are known to exist in galaxy-dense regions due to mergers and tidal stripping of galaxy gas. It is

unclear whether this explanation can be extended to the RQQs in our sample.

(iv) It is of course entirely possible that the radio properties of AGN are not determined by a single parameter but instead a combination of parameters. It is clear from previous work that for an AGN to be radio loud it requires a certain mass of black hole (McLure & Jarvis 2004) but this cannot be the only factor involved. This work and that of others (e.g. Kauffmann et al. 2008; Donoso et al. 2009) suggests that there is some link between radio loudness and the environment as well, and there have been several theoretical papers proposing that black hole spin could also be responsible.

Future observations, such as deep radio observations with the Low Frequency Array (LOFAR), will allow us to investigate the environments as a function of radio luminosity well down into the RQQ regime and up to higher redshifts, and place firmer constraints on our conclusions based on this sample alone.

ACKNOWLEDGMENTS

This work is based (in part) on observations made with the *Spitzer Space Telescope*, which is operated by the Jet Propulsion Laboratory, California Institute of Technology under a contract with NASA. Support for this work was provided by NASA through an award issued by JPL/Caltech. JTF thanks the Science and Technology Facilities Council for a research studentship. MJH thanks the Royal Society for a research fellowship. RJM acknowledges funding from the Royal Society. This research has made use of the NASA/IPAC Extragalactic Database (NED) which is operated by the Jet Propulsion Laboratory, California Institute of Technology, under contract with the National Aeronautics and Space Administration.

REFERENCES

- Adelman-McCarthy J. K. et al., 2006, *ApJS*, 162, 38
 Antonucci R., 1993, *ARA&A*, 31, 473
 Barthel P. D., 1989, *ApJ*, 336, 606
 Barthel P. D., Arnaud K. A., 1996, *MNRAS*, 283, L45
 Becker R. H., White R. L., Helfand D. J., 1995, *ApJ*, 450, 559
 Bertin E., Arnouts S., 1996, *A&AS*, 117, 393
 Best P. N., Longair M. S., Röttgering H. J. A., 1996, *MNRAS*, 280, 9
 Best P. N., Lehnert M. D., Miley G. K., Röttgering H. J. A., 2003, *MNRAS*, 343, 1
 Best P. N., Kauffmann G., Heckman T. M., Ivezić Ž., 2005, *MNRAS*, 362, 9
 Bower R. G., Benson A. J., Malbon R., Helly J. C., Frenk C. S., Baugh C. M., Cole S., Lacey C. G., 2006, *MNRAS*, 370, 645
 Bruzual G., Charlot S., 2003, *MNRAS*, 344, 1000
 Cirasuolo M., McLure R. J., Dunlop J. S., Almaini O., Foucaud S., Simpson C., 2010, *MNRAS*, 401, 1166
 Clewley L., Jarvis M. J., 2004, *MNRAS*, 352, 909
 Condon J. J. et al., 1998, *AJ*, 115, 1693
 Coppin K. et al., 2006, *MNRAS*, 372, 1621
 Croton D. J. et al., 2006, *MNRAS*, 365, 11
 Donoso E., Li C., Kauffmann G., Best P. N., Heckman T. M., 2009, preprint (arXiv:0910.3667)
 Eales S. A., 1985, *MNRAS*, 217, 149
 Ellingson E., Yee H. K. C., Green R. F., 1991, *AJ*, 378, 476
 Fan X. et al., 2003, *AJ*, 125, 1649
 Hall P. B., Green R. F., 1998, *AJ*, 507, 508
 Hardcastle M. J., Evans D. A., Croston J. H., 2007, *MNRAS*, 376, 1849
 Hill G. J., Rawlings S., 2003, *New Astron. Rev.*, 47, 373
 Hutchings J. B., Crampton D., Morris S. L., Durand D., 1999, *AJ*, 117, 1109
 Hutchings J. B., Scholz P., Bianchi L., 2009, *AJ*, 137, 3533

- Inskip K. J., Best P. N., Longair M. S., Röttgering H. J. A., 2005, MNRAS, 359, 1393
- Ivezić Ž. et al., 2002, AJ, 124, 2364
- Iverson R. J., Dunlop J. S., Smail I., Dey A., Liu M. C., Graham J. R., 2000, ApJ, 542, 27
- Jarvis M. J., McLure R. J., 2002, MNRAS, 336, L38
- Jarvis M. J., McLure R. J., 2006, MNRAS, 369, 182
- Jarvis M. J., Rawlings S., Eales S., Blundell K. M., Bunker A. J., Croft S., McLure R. J., Willott C. J., 2001, MNRAS, 326, 1563
- Kauffmann G., Heckman T. M., Best P. N., 2008, MNRAS, 384, 953
- Kukula M. J., Dunlop J. S., Hughes D. H., Rawlings S., 1998, MNRAS, 297, 366
- Lacy M., Laurent-Muehleisen S. A., Ridgway S. E., Becker R. H., White R. L., 2001, ApJ, 551, 17
- Lacy M. et al., 2005, ApJS, 161, 41
- Laing R. A., Riley J. M., Longair M. S., 1983, MNRAS, 204, 151
- Lonsdale C. J. et al., 2003, PASP, 115, 897
- McLure R. J., Dunlop J. S., 2001, MNRAS, 321, 515
- McLure R. J., Dunlop J. S., 2004, MNRAS, 352, 1390
- McLure R. J., Jarvis M. J., 2002, MNRAS, 337, 109
- McLure R. J., Jarvis M. J., 2004, MNRAS, 353, 45
- Moderski R., Sikora M., Lasota J.-P., 1998, MNRAS, 301, 142
- Pentericci L. et al., 2000, A&A, 361, L25
- Rawlings S., Jarvis M. J., 2004, MNRAS, 355, L9
- Rawlings S., Eales S., Lacy M., 2001, MNRAS, 322, 523
- Rengelink R. B. et al., 1997, A&AS, 124, 259
- Richards G. T. et al., 2006, AJ, 131, 2766
- Sadler E. M. et al., 2007, MNRAS, 381, 211
- Schneider D. P. et al., 2005, AJ, 130, 367
- Serber W., Bahcall B., Menard B., Richards G. T., 2006, AJ, 643, 68
- Sikora M., Stawarz L., Lasota J.-P., 2007, AJ, 658, 815
- Smith R. J., Boyle B. J., Maddox S. J., 2000, MNRAS, 313, 252
- Stevens J. A. et al., 2003, Nat, 425, 264
- Vardoulaki E. et al., 2010, MNRAS, 401, 1709
- Volonteri M., Sikora M., Lasota J.-P., 2007, AJ, 667, 704
- White R. L., Helfand D. J., Becker R. H., Glikman E., de Vries W., 2007, AJ, 654, 99
- Wiita P. J., 2004, Ap&SS, 293, 235
- Willott C. J. et al., 1998, in Bremer M. N., Jackson N., Perez-Fournon I., eds, ASSL Ser. Vol. 226, Observational Cosmology with the New Radio Surveys. Kluwer, Dordrecht, p. 209
- Wilson A. S., Colbert E. J. M., 1995, AJ, 438, 62
- Wold M., Lacy M., Lilje P. B., Serjeant S., 2001, MNRAS, 323, 231
- Wold M., Armus L., Neugebauer G., Jarrett T. H., Lehnert M. D., 2003, AJ, 126, 1776
- Yee H. K. C., Green R. F., 1984, AJ, 280, 79
- Yee H. K. C., Green R. F., 1987, AJ, 319, 28
- Zamfir S., Sulentic J. W., Marziani P., 2008, MNRAS, 387, 856

This paper has been typeset from a $\text{\TeX}/\text{\LaTeX}$ file prepared by the author.